Lifetimes and electromagnetic transition strengths in ^{157}Dy

K. A. Gladnishki,[1,2] P. Petkov,[2,3,4] O. Möller,[2,5] A. Dewald,[2] J. Jolie,[2] D. Tonev,[2,4] M. Trichkova,[1] S. Heinze,[2]
P. von Brentano,[2] D. Bazzacco,[6] C. A. Ur,[6] E. Farnea,[6,7] M. Axiotis,[7,8] S. Lunardi,[6] G. de Angelis,[7] D. R. Napoli,[7]
N. Marginean,[3,7] T. Martinez,[7] M. A. Caprio,[9,*] and G. Rainovski[1]

[1]*Faculty of Physics, St. Kliment Ohridski University of Sofia, 1164 Sofia, Bulgaria*
[2]*Institut für Kernphysik, Universität zu Köln, D-50937 Köln, Germany*
[3]*Horia Hulubei National Institute of Physics and Nuclear Engineering, R-76900, Bucharest-Magurele, Romania*
[4]*Bulgarian Academy of Sciences, Institute for Nuclear Research and Nuclear Energy, 1784 Sofia, Bulgaria*
[5]*Institut für Kernphysik, Technische Universität Darmstadt, D-64289 Darmstadt, Germany*
[6]*Dipartimento di Fisica and INFN, Sezione di Padova, Padova, Italy*
[7]*INFN, Laboratori Nazionali di Legnaro, Legnaro, Italy*
[8]*TANDEM Accelerator Laboratory, Institute of Nuclear Physics, NCSR "Demokritos", Athens, Greece*
[9]*Wright Nuclear Structure Laboratory, Yale University, New Haven, Connecticut 06520-8120, USA*

Lifetimes of excited states of ^{157}Dy were measured by recoil distance Doppler-shift (RDDS) and Doppler-shift attenuation (DSAM) methods. The γ-ray coincidence data were analyzed by the differential decay curve method. The level scheme and the newly deduced transition strengths were simultaneously described in the framework of the particle plus triaxial rotor model (PTRM) and the rigid-rotor model.

I. INTRODUCTION

The ^{156,157,158}Dy isotopes have neutron numbers of $N = 90$ to 92 and thus are close to the onset of prolate deformations, which takes place around $N = 88-90$ [1]. It is natural to expect a variety of collective phenomena to occur in this transitional region. Indeed, an anomalously high moment of inertia has been observed after the backbending in both the ground-state band and the β band of ^{156}Dy [2–8], while at the same time the intraband $B(E2)$ transition strengths in the first excited band (β band at lower spins and S band at higher ones) of this nucleus follow the predicted $X(5)$ behavior pattern [9,10]. It is still not clear whether the backbending phenomenon can be explained consistently just by a two-band crossing scenario involving rotational alignment of $i_{13/2}$ quasineutrons or also involves significant change in nuclear shape. At the same time, well-pronounced rotational behavior has been observed in the ground-state band of ^{158}Dy. However, it is different after the backbending as a reduced collectivity at high spin is reported [11]. This indicates a crossing with a less deformed structure. All these peculiarities suggest that the rotational behavior of these nuclei is governed by the competition between different quasiparticle configurations related to different soft and well-deformed nuclear shapes. One can speculate that the low-spin states of ^{156}Dy have partially $X(5)$-like behavior while a more deformed configuration takes over after the backbending. An opposite scenario can be surmised in the case of ^{158}Dy [11]. In this respect, it is interesting to study the rotational behavior of the odd-even nucleus ^{157}Dy. Such study requires knowledge of the electromagnetic reduced transition probabilities in the

yrast band for low- and medium-spin states. Here, we report on results from an experiment devoted to measure lifetimes of excited states of ^{157}Dy at medium and high spins.

II. EXPERIMENTAL DETAILS AND DATA ANALISIS

Two experiments (recoil distance Doppler-shift, RDDS, and Doppler-shift attenuation, DSAM) were performed using the reaction ^{124}Sn(^{36}S, $3n$) with beams provided by the XTU Tandem of the Laboratori Nazionali di Legnaro, Italy. The emitted γ rays were detected by the GASP detector array [12]. The HpGe detectors from the GASP array are grouped in seven rings with respect to the beam line. For our analysis, four rings were used where appreciable Doppler shifts can be observed, namely ring 0 (mean angle with respect to the beam axis of $34.6°$), ring 1 ($59.4°$), ring 5 ($120.6°$), and ring 6 ($145.4°$). The same setup was used in analogous lifetime measurements for excited states of ^{156,155}Dy Refs. [10,13–15]. Basic ideas about the used experimental methods can be found, e.g., in Ref. [16] and references therein (for RDDS, see also the more recent review [17]).

For the RDDS measurement, a beam of ^{36}S was accelerated to an energy of 155 MeV and then delivered to a target consisting of 0.9 mg/cm^2 tin, enriched to 97.7% in ^{124}Sn. The ^{124}Sn was evaporated onto a backing foil of 1.8 mg/cm^2 Ta. The recoiling nuclei were stopped on a 12.0 mg/cm^2 Au foil. Data have been recorded when at least two Ge detectors and two elements of the BGO inner ball fired in coincidence. The measurement was performed at 23 target-to-stopper distances. Coincident events where two γ rays are registered from detectors belonging to a particular two-ring combination were stored to γ-γ coincidence matrices for each distance. The data for different distances were normalized by using coincidence events corresponding to pairs of strong transitions (cf. also Ref. [18]). Final spectra used to determine the areas of shifted

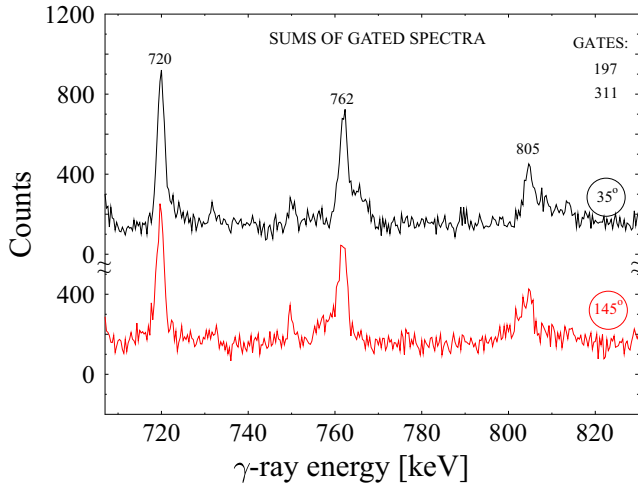*Present address: Department of Physics, University of Notre Dame, Notre Dame, Indiana 46556-5670, USA.

FIG. 1. DSAM spectra of transitions in the yrast band of ^{157}Dy obtained by setting a gate on the full γ line shape of the transitions lying below the levels of interest. The gates (γ-ray energies in keV) and the detector rings of observation are also indicated.

(γ rays emitted in flight) and unshifted (γ rays emitted in the stopper) components of transitions decaying the levels of interest were generated by setting a gate from above on the shifted component of a transition directly feeding the respective level. Equivalent gates on the same Dopper-shifted γ-rays events observed at the different rings were used. The resulting gated spectra in which the decaying transitions were observed in a certain ring were summed up. Thereby, four final spectra corresponding to the rings 0, 1, 5, and 6 were prepared for further analysis. All calibrations for energy, full width at half maximum (FWHM), and efficiency were made with a ^{152}Eu source.

For the DSAM measurement, a beam of ^{36}S accelerated to energy of 145 MeV was impinged on a 0.9 mg/cm^2 Sn enriched to 95.3% in ^{124}Sn and evaporated on a 13.4 mg/cm^2 Ta backing foil to stop the recoils. Data were recorded when at least two germanium detectors fired in coincidence. The recorded γ rays were sorted in four γ-γ matrices, with one of their axes corresponding to the energies of γ rays detected in one of the rings of interest (0, 1, 5, and 6), respectively, while the other axis being associated with energies of the coincident γ rays detected in any ring of GASP. For the further analysis, spectra were generated in the so-called gating "from below" procedure; namely, gates were set at the latter axis on the full line-shape peaks of lower lying transitions. Examples of DSAM spectra obtained in this way are shown in Fig. 1. All calibration, as for the RDDS measurement experiment, were performed by using a ^{152}Eu source.

A. Analysis of the RDDS data

The procedure described in Ref. [19] was used for extracting the lifetimes of interest from the RDDS spectra. This procedure represents a further extension of the differential decay-curve method (DDCM) [20,21] and takes into account the velocity distribution of the recoils and their finite slowdown time in the stopper. The latter adds complementary Doppler
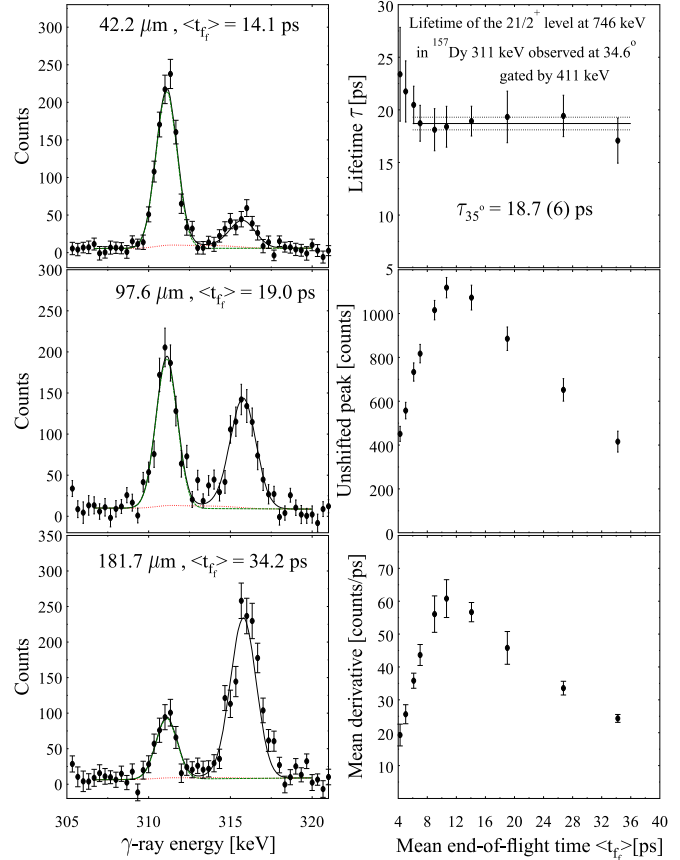

FIG. 2. Example of lifetime determination for the $21/2^+$ level in yrast band of ^{157}Dy using gated spectra measured with the detectors at $34.6°$. The gate is set on the shifted component of the 411-keV transition which directly feeds the level of interest. The left part of the figure presents fits of the line shape of the analyzed 311-keV γ-ray transition at different distances. The solid black line is the full fit. The fractions of the line shape related to the unshifted peak (dashed green line) and DSA effects (dotted red line) are shown. The right part of the figure illustrates the lifetime determination. On top, the τ curve derived is displayed together with a fit with a horizontal line within the region of sensitivity. The uncertainties of the latter are also shown. For details, see the text.

components to the line of the fully stopped peaks of γ-ray decaying states with lifetimes shorter or comparable to the stopping time of Dy ions in gold ($\sim$1.5 ps). The procedure for accounting for such contributions is described in Ref. [22]. The slowdown process and the resulting DSA contributions were modeled in a Monte Carlo simulation [23]. The electron-stopping powers were derived from the semiempirical tables of Northcliffe and Schilling [24] as described in Ref. [25]. The used nuclear stopping powers result from the LSS theory [26] after a reduction by a factor of 0.7.

An example of line-shape analysis is shown on the left-hand side of Fig. 2, where the Doppler-shift attenuated (DSA) fraction due to emissions during the slowdown is also displayed. The final value for each lifetime is determined by averaging the results obtained using all analyzed two-ring combinations. Additional corrections of the data for relativistic effects, efficiency, and solid angle effects can be neglected

TABLE I. Lifetimes and reduced electromagnetic transition probabilities in the yrast band of ^{157}Dy derived in this work from the RDDS data. The energy and the spin and parity of the corresponding level are shown in columns 1 and 2, respectively. The next column shows the energy of the depopulating γ-ray transition. In the fourth column, the derived lifetime is displayed. The reduced transition probabilities $B(E2)$ are shown in $e^2\,b^2$ and in Weisskopf units.

E_{lev} [keV]	I^π	E_γ [keV]	τ [ps]	$B(E2)$ [$e^2\,b^2$]	$B(E2)$ [W.u.]
435.6	$17/2^+$	196.9	160.5(16)	1.373(20)	272.9(39)
746.7	$21/2^+$	311.1	18.56(63)	1.426(49)	283.5(98)
1157.4	$25/2^+$	410.7	4.80(11)	1.418(33)	281.9(65)
1652.6	$29/2^+$	495.2	1.98(18)	1.362(124)	270.8(246)
2218.9	$33/2^+$	566.3	0.98(5)	1.414(72)	281.1(144)

in the present analysis. The deorientation effect was shown [27] to have no influence on results from coincidence RDDS measurements when the DDCM is used for analyzing the data.

The results derived from the analysis of the RDDS data are summarized in Table I. In total, five level lifetimes were determined in the yrast band. The lifetime of the $17/2^+$ level is determined for the first time. The obtained lifetimes are in agreement with the earlier results of Ref. [6,28] but are more precise, due to the better statistics and the use of the coincidence technique. In Fig. 3, we present as an example the analysis of the 411-keV transition as performed in ring 6 (145.4°).

B. Analysis of the DSAM data

For the DSAM analysis, the γ-ray spectra observed at angle θ can be presented as

$$S^\gamma_{ij}(E_\gamma) = \int_{-\infty}^{\infty} dE'_\gamma \frac{c}{E_{\gamma 0}} \Phi(E'_\gamma, E_\gamma)$$
$$\times \int_0^\infty dt\, P_\theta[t, v_\theta(E'_\gamma)] b_{ij} \lambda_i n_i(t). \quad (1)$$

The detailed description of the equation can be found in Ref. [14]. Specific corrections related to the present experimental geometry, angular correlations, and kinematic effects (cf. Ref. [16]) are also included in Eq. (1).

The approach which was used for analyzing single DSA line shapes and deriving lifetimes is presented in Refs. [21,25]. For the calculation of the matrix $P_\theta(t, v_\theta)$, which describes the stopping process, we used a modified version of the computer code DESASTOP [29,30] by Winter. This version allows for a numerical treatment of the electron stopping powers at relatively higher ion energies (see Ref. [14]). To determine the numerical electron stopping power for ^{157}Dy ions in the target and stopper materials, an interpolation from tabulated data [24] was utilized. The influence of the atomic structure of the medium was accounted for by introducing an additional correction as described in Refs. [31,32]. This correction accounts for deviations from the relatively smooth dependence on Z predicted by the Northcliffe and Schilling tables [24]. For adjustment of the electron stopping power of the Sn target,
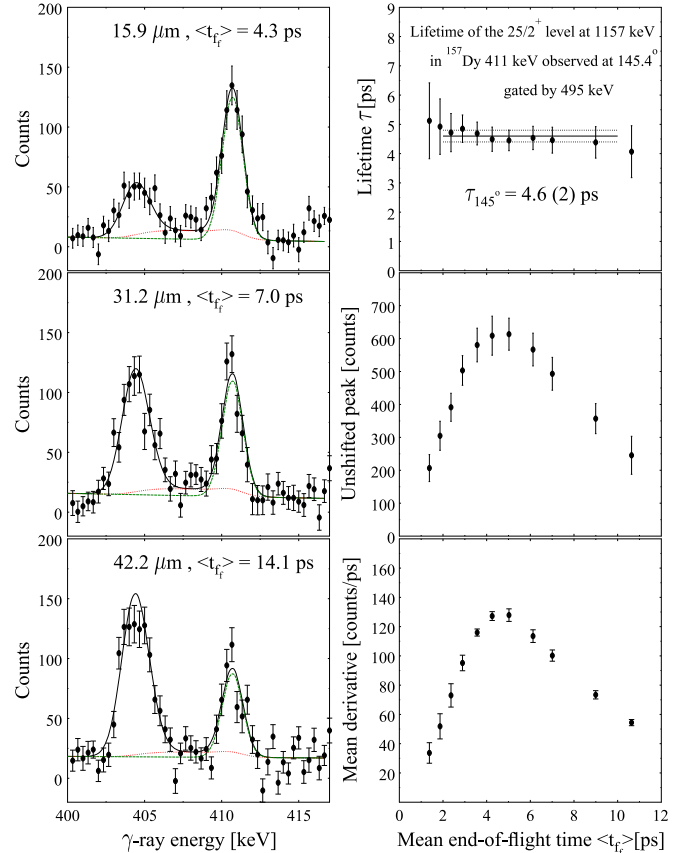

FIG. 3. The same as in Fig. 2 but for the 411-keV transition, which depopulates the $25/2^+$ level. The gated spectra are measured with the detectors at 145.4°.

we used the RDDS measurement, namely the line shapes of the shifted peaks at large distances which are representative for the velocity distribution of the recoils leaving the target. The nuclear stopping process was modeled according to the Lindhard, Scharff, and Schiøtt (LSS) theory [26] and the parametrization of the universal scattering function for a Thomas-Fermi potential given in Ref. [23]. The effect of microchanneling in the stopping medium was corrected via reduction of the nuclear stopping power by a factor $f_n = 0.7$ (cf. Refs. [31,33] for more details).

In order to obtain the line shapes of the investigated γ-ray transitions, gates were set in the γ-γ coincidence matrices on fully stopped peaks of lower-lying γ-ray transitions. Four line shapes (at the four different ring angles) for each transition of interest were obtained and analyzed independently according to the procedure outlined in detail in Refs. [21,25]. In the left-hand side of Fig. 4, the procedure is illustrated for the 762-keV transition in the yrast band.

The line-shape analysis yields the decay functions of the level of interest i. This function and the one for the preceding, higher lying levels h are used to determine the lifetime τ according to the differential decay-curve method (DDCM) [20] in the case of DSAM measurements [21]:

$$\tau_i(t) = \frac{-\lambda_i \int_0^t dt' n_i(t') + \sum_h b_{hi} \lambda_h \int_0^t dt' n_h(t')}{\lambda_i n_i(t)}, \quad (2)$$
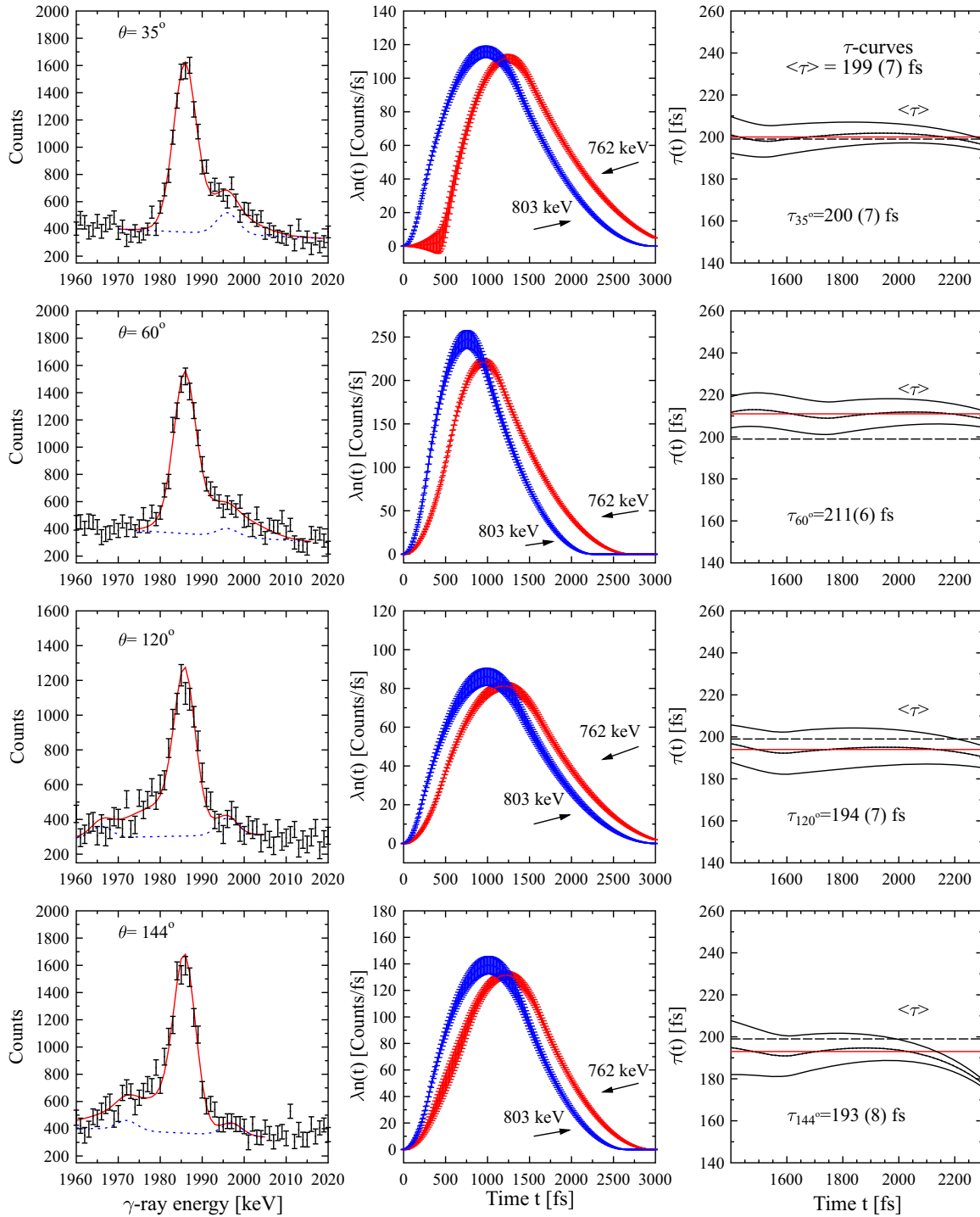
FIG. 4. The line-shape analysis of the 762-keV transition from yrast band of ^{157}Dy (Ii → If transition) and extraction of the lifetime of the $I^\pi = 49/2^+$ level at 5004.1 keV [cf. Eq. (2)]. On the left-hand side are shown fits of the line shapes measured at the angles of 35°, 59°, 121°, and 145° with respect to the beam axis. Dashed lines show the background as well as small contaminant peaks. The decay functions are presented in the middle with their statistical uncertainties. The decay function of the feeding transition of 803 keV is also shown as determined. It is determined independently and its area is normalized to that of the decay function of the 762-keV transition. The τ curves and their statistical uncertainties are presented on the right-hand side. The lifetimes τ_θ derived at the four detector angles and their statistical errors are also displayed. The final adopted value of the lifetime is $\langle\tau\rangle = 199 \pm 7$ fs.

where the summation over h includes all direct feeders of the level i.

Because the line shapes are analyzed in spectra generated by setting a gate on lower lying transitions, care is taken

to account for the influence of unknown side feeding on the extracted lifetimes. For this purpose, we adopted the often-used hypothesis that the lifetime of the unknown feeding is the same as that of the known one. Examples of τ curves

TABLE II. Lifetimes and reduced electromagnetic transition probabilities in ^{157}Dy derived in this work from the DSA data. In columns 1 and 2, the energy and spin of the levels investigated are shown, respectively. The energies of the analyzed depopulating γ-ray transitions are presented in column 3. In the fourth column, the derived lifetime is displayed. The reduced transition probabilities $B(E2)$ are shown in $e^2\,b^2$ and in Weisskopf units.

E_{lev} [keV]	I^π	E_γ [keV]	τ [fs]	$B(E2)$ [$e^2\,b^2$]	$B(E2)$ [W.u.]
3521.2	$41/2^+$	676.4	425.8(306)	1.344(94)	267.2(190)
4241.8	$45/2^+$	720.6	275.0(180)	1.518(100)	301.8(198)
5004.1	$49/2^+$	762.3	198.5(70)	1.589(57)	315.8(112)
5806.9	$53/2^+$	802.8	179.2(94)	1.341(71)	266.6(141)

obtained for the 762-keV transition in the yrast band at the four detector angles are shown in Fig. 4 on the right-hand side. The decay functions used for the calculation of the values of the τ curves are displayed in the middle of this figure. The weighted average values τ_θ within the sensitivity region and their statistical uncertainties $\Delta\tau_\theta$ were calculated using error propagation and taking into account the correlations between the different quantities in Eq. (2). The final result for τ was obtained as an unweighted mean of the values determined independently at the different rings. For the uncertainty of its value, we adopted the square root of the variance of the results obtained at the four different rings.

The analysis of the DSA data yields four lifetimes in the yrast band of ^{157}Dy, summarized in Table II. The lifetimes of the $49/2^+$ and the $53/2^+$ levels were determined for the first time. The obtained lifetimes are in agreement with the earlier results of Refs. [6,28] but are more precise due to the better statistics and the use of the coincidence technique.

III. DISCUSSION

The new experiments provide full information on the electromagnetic properties of the ground-state band. This allows the properties of the rotational behavior of ^{157}Dy to be understood more thoroughly. To describe the yrast band at low spins in the present work, we used the particle plus triaxial rotor model (PTRM) described in Ref. [34] and implemented in the computer codes GAMPN, ASYRMO, PROBAMO, and E1PROBAM presented in Refs. [35,36]. The version of the PTRM used in this work accounts for the quadrupole deformation of the core and of the complex structure of the physical states built by the contributions of different single-quasiparticle orbitals. The performed PTRM calculations are analogous to the ones described in Ref. [14] where more details of utilizing the model are presented. Here, we restrict ourselves to a brief description of the model's parameters used in the present study.

The model used a set of Nilsson orbitals which are generated for certain initial deformation parameters ϵ, γ, and ϵ_4. From these states, the particle plus rotor strong-coupling basis for a given parity is constructed. In this basis, all single-particle matrix elements necessary for the particle plus

TABLE III. Squared amplitudes of the of the different Nilsson orbitals in the PTRM wave functions for the states in the ground-state band.

Spin [$\hbar$]	$1/2^+[660]$	$3/2^+[651]$	$5/2^+[642]$	$7/2^+[633]$
1/2	100			
5/2	54	43	3	
7/2	9	73	17	0.3
9/2	57	37	6	
11/2	9	64	26	1
13/2	58	35	7	0.3
15/2	8	59	31	3
17/2	59	34	8	0.5
19/2	8	55	34	4
21/2	59	33	8	0.7
23/2	7	51	36	6
25/2	59	32	8	0.9
27/2	7	49	37	7
29/2	58	32	9	1

rotor Hamiltonian and the calculation of transition strengths are computed. In this approach to the pairing, the Fermi level and the pairing gap are derived quantities, although the codes used by us offer the possibility to treat them as adjustable parameters. In our calculations, we used 15 orbitals lying closest to the Fermi level for each parity. The pairing BCS calculation yielded a Fermi level $\lambda = 51.56$ MeV and a pairing gap $\Delta = 1.03$ MeV. To describe the spectrum of the excitation energies and the transition strengths, we varied ϵ, γ, and ϵ_4 as well as the excitation energy $E(2_1^+)$ of the 2_1^+ state of the core and the attenuation ζ of the Coriolis interaction. In this way, a search for the best set of deformation parameters which describe the data was performed. In the present work, deformation parameters for the best description of the experimental data were found to be $\epsilon = 0.26$, $\gamma = 0°$, and $\epsilon_4 = 0.0$, which ensured a reasonable reproduction of the positions of the bandheads observed at lower spin in ^{157}Dy and of the intraband $B(E2, I \rightarrow I - 2)$ values. The final results for the calculated level scheme were obtained by a fine tuning of the moments of inertia and the attenuation of the Coriolis interaction. They were fixed by the values $E(2_1^+) = 0.085$ MeV, $\zeta^{\pi=+} = 0.8$, and $\zeta^{\pi=-} = 0.7$. For the calculations of $M1$ transition strengths and magnetic moments, the neutron g_s factor was reduced to 0.7 of its free value and the core factor g_R was fixed to Z/A.

The comparison of the results of the PTRM calculations to the experiment are shown in Fig. 5. An overall agreement is observed. Both model calculations and the experimental results show no indications for a reduction of the collectivity in the yrast band with increasing spin.

The yrast band in ^{157}Dy has two signatures. In Table III, we present the PTRM wave functions decomposed in the Nilsson basis. The wave functions of both signatures are mostly dominated by the low-Ω $1/2^+[660]$, $3/2^+[651]$, and $5/2^+[642]$ orbitals. The $1/2^+[660]$ and the $3/2^+[651]$ orbitals dominate the wave functions of the favored signature while in the wave functions of the unfavored signature the contribution of the
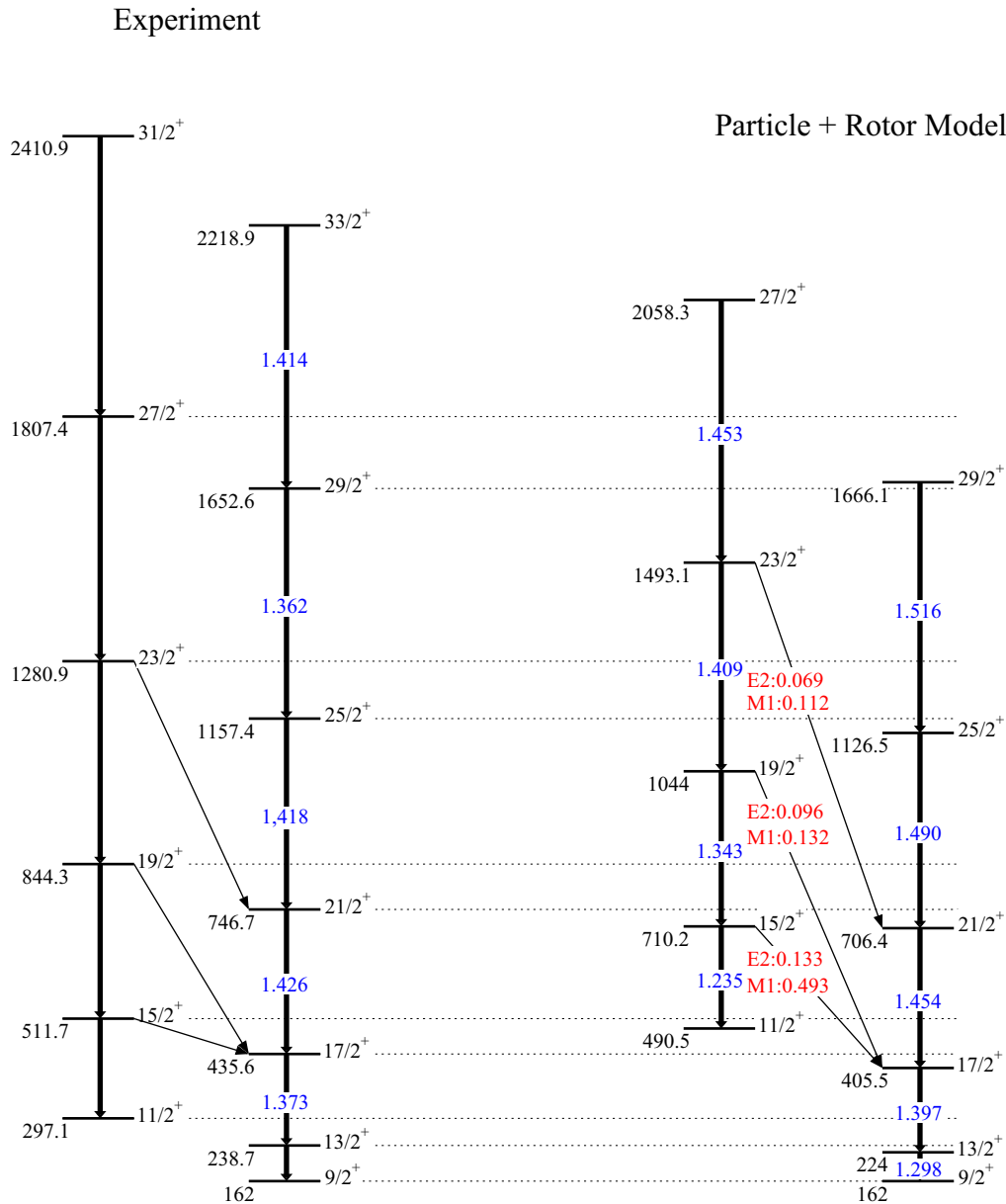
FIG. 5. Comparison of the experimental and calculated within the PTRM level schemes of ^{157}Dy. The numbers on the arrows of the $\Delta I = 2$ transitions are the $B(E2)$ values in units e^{2}b^2. For the theoretical $\Delta I = 1$ transitions of mixed multipolarity, the $B(E2)$ values are given in e^{2}b^2 (top) and the $B(M1)$ values are in μ_N^2 (bottom). See also text.

$1/2^+$[660] is strongly reduced at the expense of $5/2^+$[642] orbital. This reduction is the reason for the relatively smaller calculated $B(E2)$ values in the unfavored signature (cf. Fig. 5).

Assuming that at higher spin the deformation parameters do not change dramatically, one can expect that the overall behavior of the $B(E2)$ values as a function of spin should be reproduced in the framework of the semiclasical rigid rotor model [37]. Though limited, this approach could indicate to what extent the rotational behavior of ^{157}Dy for higher spins

is due to changes of the deformation of a soft core. To check that hypothesis, we calculated the $E2$ transition strengths by using

$$B(E2, I \rightarrow I - 2) = \frac{5}{16\pi} e^2 Q_0^2 \langle I K 2 0 | I - 2 K \rangle^2. \quad (3)$$

For the intrinsic quadrupole moment, a value of $Q_0 = 6.51$ eb is assumed [38]. Two different values of the projection $K = \Omega$ of the angular momentum on the symmetry axis were considered in accordance to the results from the wave
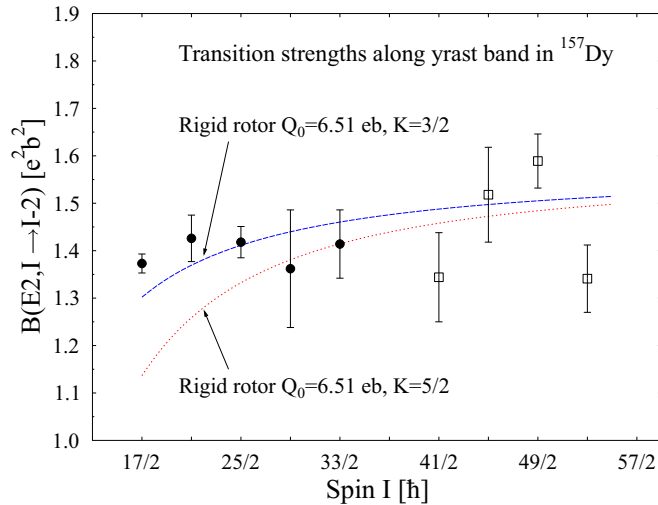
FIG. 6. Reduced $B(E2, I \rightarrow I - 2)$ transition strengths in the yrast band. The results of the RDDS (filled circles) and the DSAM measurements (open squares) are presented together and compared to the results from the rigid-rotor model with the indicated parameters.

functions analysis in the PTRM. The comparison between the calculated and the experimental $B(E2)$ values (see Fig. 6) shows qualitative agreement up to spin $I^\pi = 53/2^+$, indicating that the nuclear shape at higher spins remains stable and similar to the one for the ground-state band.

IV. SUMMARY

In the present work, RDDS and DSAM lifetime measurements were carried out. Nine lifetimes were determined, three of them for the first time. The experimental data on the level energies and the deduced transition strengths were compared to the results of particle plus triaxial rotor model and rigid-rotor calculations. Both models, within their limits, describe the experimental data reasonably well. This indicates that in ^{157}Dy, the addition of one odd neutron to the soft even-even core ^{156}Dy stabilizes the nuclear shape.

[1] R. F. Casten, D. D. Warner, D. S. Brenner, and R. L. Gill, Phys. Rev. Lett. **47**, 1433 (1981).

[2] R. M. Lieder, H. Beuscher, W. F. Davidson, A. Neskakis, C. Mayer-Böricke, Y. El Masri, P. Monseu, J. Steyaert, and J. Vervier, Phys. Lett. B **49**, 161 (1974).

[3] H. R. Andrews, D. Ward, R. L. Graham, and J. S. Geiger, Nucl. Phys. A **219**, 141 (1974).

[4] D. Ward, H. R. Andrews, O. Haüsser, Y. El Masri, M. M. Aléonard, I. Yang-Lee, R. M. Diamond, F. S. Stephens, and P. A. Butler, Nucl. Phys. A **332**, 433 (1979).

[5] Y. El Masri, J. M. Ferté, R. Janssens, C. Michel, P. Monseu, J. Steyaert, and J. Vervier, Nucl. Phys. A **271**, 133 (1976).

[6] H. Beuscher, W. F. Davidson, R. M. Lieder, A. Neskakis, C. Mayer-Böricke, Nucl. Phys. A **249**, 379 (1975).

[7] A. W. Sunyar, in *Proceedings of the Symposium on Highspin Phenomena in Nuclei* (Argonne National Laboratory, Argonne, IL, 1979), ANL/PHY-79-4, p. 77.

[8] P. Thieberger, A. W. Sunyar, P. C. Rogers, N. Lark, O. C. Kistner, E. der Mateosian, S. Cochavi, and E. H. Auerbach, Phys. Rev. Lett. **28**, 972 (1972).

[9] F. Iachello, Phys. Rev. Lett. **87**, 052502 (2001).

[10] O. Möller, A. Dewald, P. Petkov, B. Saha, A. Fitzler, K. Jessen, D. Tonev, T. Klug, S. Heinze, J. Jolie *et al.*, Phys. Rev. C **74**, 024313 (2006).

[11] H. Emling, E. Grosse, D. Schwalm, R. S. Simon, H. J. Wollersheim, D. Husar, and D. Pelte, Phys. Lett. B **98**, 169 (1981).

[12] D. Bazzacco, in *Proceedings of the International Conference on Nuclear Structure at High Angular Momentum*, (Ottawa, Canada, 1992), Chalk River Report No. AECL 10613, p. 386.

[13] P. Petkov, A. Dewald, C. Möller, B. Saha, A. Fitzler, K. Jessen, D. Tonev, T. Klug, S. Heinze, J. Jolie *et al.*, Phys. Rev. C **68**, 034328 (2003).

[14] P. Petkov, M. S. Yavahchova, O. Möller, A. Dewald, D. Tonev, B. Saha, A. Fitzler, K. Jessen, T. Klug, S. Heinze *et al.*, Phys. Rev. C **88**, 034323 (2013).

[15] M. Yavahchova, P. Petkov, A. Dewald, C. Möller, B. Saha, A. Fitzler, K. Jessen, D. Tonev, N. Gutev, T. Klug *et al.*, J. Phys.: Conf. Ser. **366**, 012050 (2012).

[16] T. K. Alexander and J. S. Forster, Adv. Nucl. Phys. **10**, 197 (1978).

[17] A. Dewald, O. Möller, and P. Petkov, Prog. Part. Nucl. Phys. **67**, 786 (2012).

[18] A. Dewald, P. Sala, R. Wrzal, G. Böhm, D. Lieberz, G. Siems, R. Wirowski, K. O. Zeil, A. Gelberg, P. von Brentano *et al.*, Nucl. Phys. A **545**, 822 (1992).

[19] P. Petkov, D. Tonev, J. Gableske, A. Dewald, T. Klemme, and P. von Brentano, Nucl. Instr. Meth. Phys. Res. A **431**, 208 (1999).

[20] A. Dewald, S. Harissopulos, and P. von Brentano, Z. Phys. A **334**, 163 (1989).

[21] G. Böhm, A. Dewald, P. Petkov, and P. von Brentano, Nucl. Instr. Meth. Phys. Res. A**329**, 248 (1993).

[22] P. Petkov, D. Tonev, J. Gableske, A. Dewald, and P. von Brentano, Nucl. Instr. Meth. Phys. Res. A**437**, 274 (1999).

[23] W. M. Currie, Nucl. Instr. Meth. **73**, 173 (1969).

[24] L. C. Northcliffe and R. F. Schilling, Nucl. Data, Sect. 7, 233 (1970).

[25] P. Petkov, J. Gableske, O. Vogel, A. Dewald, P. von Brentano, R. Krücken, R. Peusquens, N. Nicolay, A. Gizon, J. Gizon *et al.*, Nucl. Phys. A **640**, 293 (1998).

[26] J. Lindhard, M. Scharff, and H. E. Schiøtt, Kgl. Dan. Vid. Selsk. Mat. Fys. Medd. **33**, 14 (1963).

[27] P. Petkov, Nucl. Instr. Meth. Phys. Res. A **349**, 289 (1994).

[28] H. Emling, E. Grosse, R. Kulessa, D. Schwalm, and H. J. Wollersheim, Nucl. Phys. A **419**, 187 (1984).

[29] G. Winter, ZfK Rossendorf Report ZfK-497, Rossendorf, 1983.

[30] G. Winter, Nucl. Instr. Meth. **214**, 537 (1983).

[31] J. F. Ziegler and J. P. Biersack, in *Treatise on Heavy-Ion Science*, edited by D. A. Bromley (Plenum Press, New York, 1985), Vol. 6, p. 95.

[32] J. F. Ziegler and W. K. Chu, At. Data Nucl. Data Tables **13**, 463 (1974).

[33] J. Keinonen, in *Capture Gamma-Ray Spectroscopy and Related Topics-1984, Proceedings of the Fifth International Symposium, Knoxville, Tennessee*, AIP Conf. Proc. No. 125, edited by S. Raman (AIP, New York, 1985), p. 557

[34] S. E. Larsson, G. Leander, and I. Ragnarsson, Nucl. Phys. A **307**, 189 (1978).

[35] I. Ragnarsson and P. B. Semmes, Hyp. Int. **43**, 423 (1988).

[36] P. B. Semmes, Computer manual, presented at Nuclear Structure Theory Workshop, Oak Ridge, TN, 1991 (unpublished).

[37] A. Bohr and B. R. Mottelson, *Nuclear Structure* (Benjamin, New York, 1975), Vol. 2.

[38] A. Bohr and B. R. Mottelson, Dan. Mat.-Fys. Medd. **30**, 1 (1955).